

PHYSICS AND ENGINEERING ASPECTS  
OF THE  
OAK RIDGE EXPERIMENTAL POWER REACTOR\*

D. C. McAlees  
Exxon Nuclear Co., Inc.  
Bellevue, Washington 98009

and

E. S. Bettis, T. J. Huxford, F. B. Marcus  
R. T. Santoro, H. L. Watts  
Oak Ridge National Laboratory  
Oak Ridge, Tennessee 37830

Conf-751125--61

By acceptance of this article, the publisher or recipient acknowledges the U.S. Government's right to retain a nonexclusive, royalty-free license in and to any copyright covering the article.

**NOTICE**  
This report was prepared as an account of work sponsored by the United States Government. Neither the United States nor the United States Energy Research and Development Administration, nor any of their employees, nor any of their contractors, subcontractors, or their employees, makes any warranty, express or implied, or assumes any legal liability or responsibility for the accuracy, completeness or usefulness of any information, apparatus, product or process disclosed, or represents that its use would not infringe privately owned rights.

Summary

The first tokamak experimental power reactor (EPR) is planned for operation in the mid-1980's. The logic leading to the size of the ORNL reference reactor, the technical features of the plasma and energy conversion systems, and the predicted parameters consistent with several operating modes are discussed in this paper. The mechanical aspects of the blanket and shield systems and an evaluation of their nuclear performance including tritium breeding, nuclear heating and radiation damage are also given.

Plasma System Parameters

All of the objectives for the EPR lead to the requirement that fast-charged particles, both fast ions due to injection and thermonuclear-produced alpha particles, be efficiently contained within the plasma volume. The device must be large enough to contain the drift orbits followed by these particles. This in turn suggests a high value of plasma current. The current is given by,

$$I = \frac{2\pi B_{\max}}{\mu_0 q} \frac{1}{A^2} \left[ (A - 1) a - \Delta \right], \quad (1)$$

where  $B_{\max}$  is the toroidal field strength at the coil winding,  $q$  is the stability factor,  $A$  is the aspect ratio,  $a$  is the plasma radius and  $\Delta$  is the radial distance from the surface of the plasma to the surface of the toroidal field coil winding. For a given plasma radius,  $I$  is relatively insensitive to the aspect ratio,  $A$ . Qualitatively, the distance  $\Delta$  must include the blanket and shield thickness, insulation, and the necessary tolerances to permit remote assembly and disassembly of these components. Quantitatively,  $\Delta \approx 1.5$  m. for a power-producing device with  $a \approx 2$  m. which is the physical size anticipated for an EPR plasma. The minimum acceptable value of  $q(a)$  depends on the radial distribution of plasma current density. Finally, the maximum toroidal field strength chosen must be compatible with the expectations for advances in superconducting technology. These criteria and the requirements of long pulse time, a compatible neutral beam system and an acceptable value for the toroidal field ripple<sup>1</sup> result in the choice of the ORNL-EPR plasma-related parameters as shown in Table I.

Table I

EPR-1 Reference Parameters  
Plasma Subsystem Requirements

Plasma radius, $a$ (m)	2.25
Major radius, $R_0$ (m)	6.75
Safety factor, $q(a)$	2.5
Maximum toroidal field, $B_{\max}$ (T)	11.
Toroidal field on axis, $B_T$ (T)	4.8
Plasma Current, $I$ (MA)	7.2
Plasma edge to winding distance, $\Delta$ (m)	1.55
Volt-second, (V·s, Wh)	185
Injection power capability, $P_b$ (MW)	50
Deuteron energy, $E_b$ (keV)	200
Number of Injectors, $N_I$	6
Number of toroidal coils, $N_c$	20
Toroidal field ripple, $\delta(0 < r < a)$	2.2%

Plasma Performance

The scaling laws which ultimately will apply to EPR-size plasmas are presently uncertain. A simulation model which is time dependent and includes dissipative trapped particle diffusion, pseudoclassical and neoclassical diffusion, conduction and convection losses, impurity effects, radiation, coil fueling, and neutral beam injection effects has been used to model the plasma behavior. The reference plasma described here assumes that the dissipative trapped particle diffusion terms are a factor of 10 more optimistic than those given in reference (2). Figure 1 shows the startup phase and approach to equilibrium for the reference system described above.  $P_F^M$  and  $P_F^{b-P}$  are the Maxwellian or background and beam-plasma produced fusion power levels, respectively.  $P/S$  is the neutron wall loading. The plasma ignites in  $\sim 5$  s.

In this operating mode the total fusion power is 225 MW immediately before ignition and 175 MW after the beams are terminated at ignition. The neutron wall loading is about  $0.2 \text{ MW/m}^2$ , the ion temperature is 9 keV and  $N_e T_e = 6 \times 10^{14} \text{ cm}^{-3}\text{-s}$ . In this case  $P \approx \sqrt{A}$ .

If a  $B \approx A$  could be tolerated, the same system could be operated differently and at a significantly higher power level. Figure 2 shows the ion temperature as a function of time for an operating mode where the system is initially impurity free

\*Research sponsored by the Energy Research and Development Administration under contract with Union Carbide Corporation.

**MASTER**

and neutron, charged particle and chemical sputtering occur during the pulse. The characteristic temperature of the particles interacting with the wall is assumed to be  $0.05 \langle T_i \rangle$  or 5 percent of the average ion temperature. The fraction of the sputtered particles returning to the plasma and their containment time in the plasma are given by  $f_s$  and  $\tau_c$ , respectively.

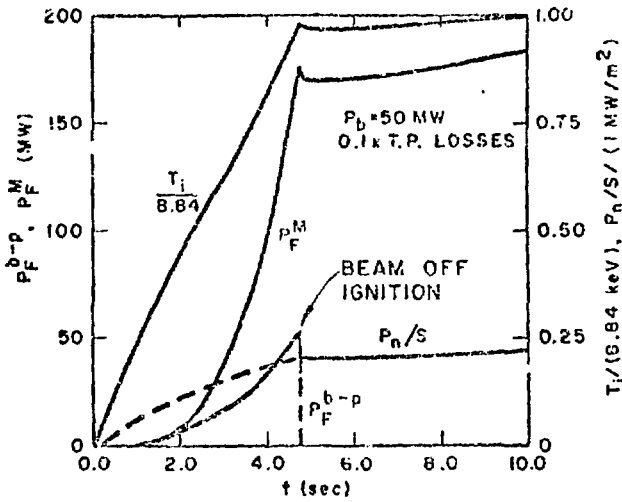


Figure 1

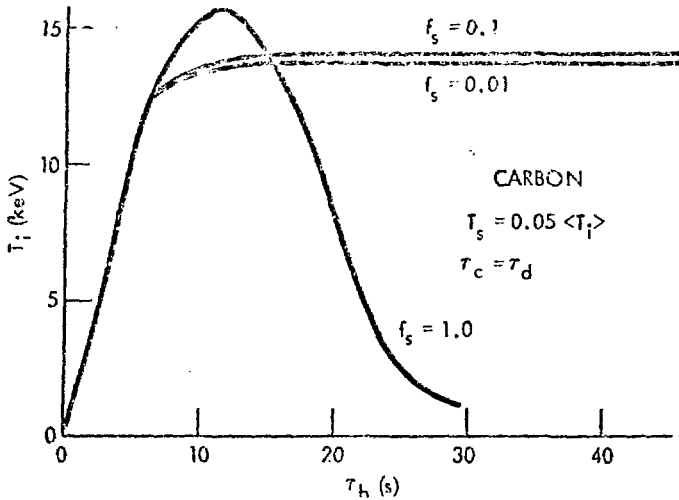


Figure 2

The chemical sputtering yield<sup>3</sup> is assumed to be constant (0.03), the charged particle sputtering yields are energy dependent<sup>4</sup> and in the same ratios as those given by Behrisch<sup>5</sup> for Nb. The absolute values are normalized to that taken for deuterons (0.04). For the long burning cases shown in Figure 2,  $P_F \approx 800$  MW,  $\beta_p \approx 2.7$ , and  $P_n/S = 1$  MW/m<sup>2</sup>. This case results in  $P_b = 160$  MW, or 160 MW of heat loss which must be removed by cooling the first wall.

### Blanket and Shield System

The philosophy used to develop the reference blanket design was that its features must be consistent with extrapolation to a fusion reactor. This restraint coupled with the requirements of useful heat production, compatibility with remote assembly, and the need to demonstrate tritium breeding in at least one module resulted in the design shown in Figure 3.

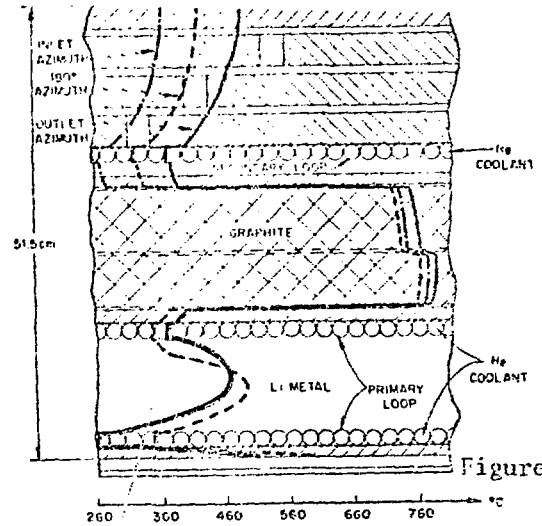


Figure 3

There are 60 blanket segments which, when clamped together and seal-welded, comprise the plasma vacuum enclosure. These segments are wedge shaped and are 95 centimeters wide on the outer circumference and about 40 centimeters wide on the inner circumference. The size of the segments allows them to be loaded between the toroidal field coils thus permitting removal of any or all segments for maintenance without interfering with the coils. Totally remote techniques would be used in the assembly and disassembly procedures.

All structure is 316 stainless steel, and the principle neutron absorber material is liquid metal. For the experimental breeding modules, lithium is used. For the non-breeding modules either sodium or potassium is used. The blanket is cooled by helium at a pressure of 70 atmospheres. The helium inlet temperature is 260° C and the outlet temperature is 371° C.

The blanket section (See Figure 3) is composed of three basic regions inside of a stainless steel, wedge-shaped, circular structure. The first region, which contains liquid metal is 25 centimeters thick. This section absorbs about 52% of the neutron and gamma-ray energy produced. In the case of the breeding module, it produces most of the tritium. The first two rows of coolant tubes are in series so that the coolant first passes near the inner wall to remove the heat deposited there by plasma loss processes. The helium then flows through the second row of tubes and into the outlet header. The liquid metal conducts the heat from the first wall structure to the coolant tubes.

The second region is 10 centimeters thick and is composed of graphite. This reflector moderates and scatters the fast neutrons so that a high fraction of them return to the lithium. The slower neutrons are captured by <sup>6</sup>Li in the breeding modules. This graphite reflector is cooled by radiation from all faces to the cooler portions of the blanket.

The third region is the gamma-ray shield which consists of concentric stainless steel shells with about 0.5 centimeters of liquid metal between them. A third row of coolant tubes is included to remove heat from the shield. Again, the liquid metal provides a conduction path to the tubes.

The blanket design is presently capable of performing under the operating conditions shown on Figure 1. In the high power mode (cf. Figure 2) or a beam driven mode, the plasma losses approach 160 MW; and the neutron loading is  $< 640 \text{ MW}$ . This is the most severe case of EPR operation presently visualized. For this case the thermal stress in the first wall is too high. This problem will be solved by changing the blanket first wall from a slab geometry to a structured wall.

The temperatures, pressures, pumping power, and other thermal-hydraulic parameters for this blanket concept when it is operated in the driven mode (plasma losses are 160 MW and neutron loading is 240 MW) are shown in Table II.

Table II

Results of Thermal-Hydraulic Calculations for the EPR Reference Blanket Design

Fusion Power, MW(th)	300.
Neutral Beam Power to Plasma, MW(th)	100.
Total Power from Plasma, (Losses and Fusion) MW(th)	400.
Heat Deposited, First Wall MW/m <sup>2</sup>	0.27
Neutron Wall Loading MW/m <sup>2</sup>	0.40
Helium Flow Rate, Kg/s	658.
Helium Inlet Temperature, °C	260.
Helium Outlet Temperature, °C	371.
Helium Pressure, atm	70.
Helium Pumping Power, MW; % Output	22.; 5.5
Max. Temp. in Graphite Curtain, °C	1,779.
Max. Temp. in SS. Blanket Structure, °C	604.
Max. Temp. in Lithium, °C	502.
Max. Temp. in Graphite Reflector, °C	789.

Helium Tube Bank	1	2	3
Cooling Surface Area, m <sup>2</sup>	1523.	1673.	1772.
Average Gas Velocity, m/s	76.	83.	22.
Surface Heat Flux, w/cm <sup>2</sup>	16.	5.	3.

#### Nuclear Performance

All of the neutronics calculations were carried out using the one-dimensional discrete ordinates code ANJISN,<sup>6</sup> using a P<sub>3</sub> scattering expansion, an S<sub>12</sub> quadrature, and the coupled neutron-gamma-ray cross-section library (100 n - 21 γ) of Plaster, Santoro, and Ford.<sup>7</sup> Energy deposition in the reactor was estimated using coupled neutron-photon kerma factors obtained from MACRLIB<sup>8</sup> and SMOG,<sup>9</sup> respectively. Radiation damage was calculated using the displacement cross sections of Gabriel, Amburgey, and Green<sup>10</sup> and (n,p) and (n,α) reaction cross sections from ENDF/B-4.

The nuclear performance of the EPR reference design was estimated using the configuration shown in Figure 4 and previously described. Due to the numerous operating modes possible, a standard case of 100 MW source neutron wall loading ( $\sim 0.2 \text{ MW/m}^2$ )

was used here. Also, iron was taken to be the structural material recognizing that, in practice, a stainless-steel alloy or refractory metal alloy will probably be used.

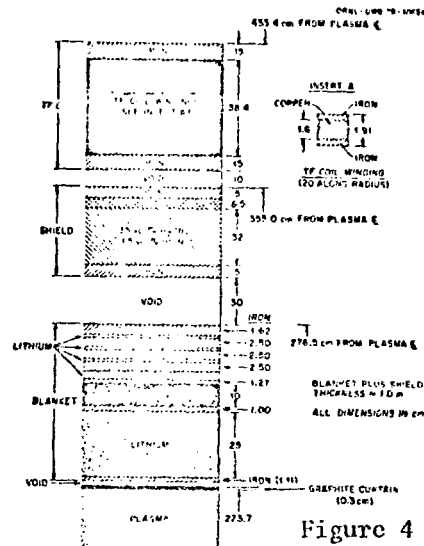


Figure 4

The neutron flux is reduced by a factor of 7 in passing through the blanket and is further reduced by a factor of the order of 700 in passing through the shield. The blanket and the shield combine to produce a neutron attenuation of approximately 4900.

Although tritium breeding is not a major requirement for the EPR, it must be demonstrated in a few breeding blanket modules. In the calculations and as shown in Figure 4, natural lithium is used as the breeding material. The total breeding in the reference design is 1.213 tritium nuclei per incident neutron. The contributions to the total breeding from <sup>6</sup>Li and <sup>7</sup>Li in the several zones are summarized in Table III.

Table III

Tritium Breeding Ratio

Zone	Description	Tritium Nuclei Incident Neutron		
		R <sub>6</sub> Li	R <sub>7</sub> Li	Total
5	25-cm Absorber	0.619	0.434	1.053
9	2.5-cm Absorber	0.111	0.007	0.118
11	0.5-cm Absorber	0.016	0.001	0.017
13	0.5-cm Absorber	0.013	0.0005	0.014
15	0.5-cm Absorber	0.012	0.0003	0.012
Total		0.771	0.443	1.213

Since the EPR is being designed to produce electrical power, the blanket must absorb a sufficient fraction of the fusion neutrons and secondary gamma rays so that the blanket coolant temperature can be raised high enough to permit efficient conversion to electrical power. The energy-deposition rate as a

function of radial distance from the plasma center is shown in Figure 5.

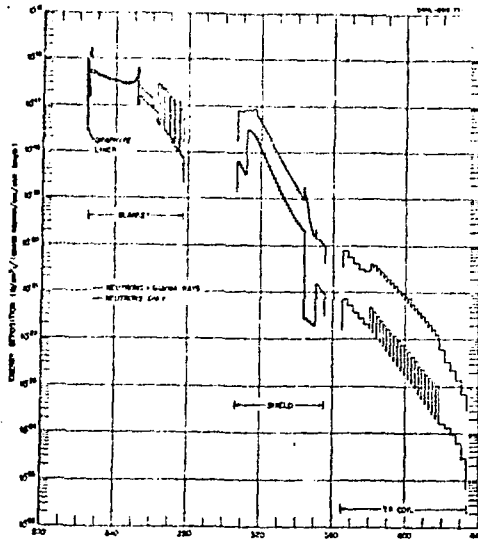


Figure 5

Note that the abscissa is offset by 200 cm. The solid curve shows the radial dependence of the heating due to neutrons and gamma rays and the curve bearing the tick marks shows the radial dependence of the heating from neutrons only. The heat deposition occurs predominantly in the blanket followed by a somewhat rapid reduction in the heating through the shield. The effectiveness of the iron and the lead layers in the shield in attenuating gamma rays generated in both the blanket and the shield and converting them to heat in the shield rather than in the cryogenic TF coil is shown clearly in the large differences between the two curves for these materials. The structure in the two curves in the TF coil region shows the contributions to local heating from the copper coil windings and their iron enclosures.

The total fraction of energy deposited in the blanket assembly is 89.8%, which is consistent with the design specification for 90% energy deposition in the blanket. The graphite curtain and the shield absorb 10.1% of the total heat, and the remainder (<< 0.1%) is absorbed in the TF coil assembly.

Estimates of the radiation damage in the first iron wall and in the first copper winding in the TF coil are given in Table IV.

Table IV  
Estimates of Radiation Damage

dpa/year	Hydrogen Atoms cm <sup>3</sup> /year	Helium Atoms cm <sup>3</sup> /year
	<u>First Iron Wall</u>	
1.89	4.73 x 10 <sup>18</sup> (56 appm)	1.47 x 10 <sup>18</sup> (18 appm)

First Copper Winding  
in TF Coil

4.20 x 10<sup>-5</sup>      3.75 x 10<sup>12</sup>      8.71 x 10<sup>11</sup>

These results are continuous operation for one year at a source neutron wall loading of 0.168 MW/m<sup>2</sup>. The displacement cross sections used in arriving at these values have thresholds of 40 eV for iron and 30 eV for copper. At the assumed power level, the atomic-displacement rate and the gas-production rate are low and do not represent a significant level of damage to either the first iron wall and, most certainly, to the copper windings in the TF coil.

If these data are extrapolated to a wall loading of 1.0 MW/m<sup>2</sup>, the atomic-displacement rate is 11.25 dpa/y, a value that is consistent with the rates predicted by Kulcinski, Doran, and Abdou<sup>11</sup> and by Williams, Santoro, and Gabriel.<sup>12</sup> It should be noted that in both References 11 and 12 stainless-steel alloys rather than just iron were used in calculating the dpa rates. Correspondingly, the hydrogen- and helium-production rates in the first iron wall increase to 2.82 x 10<sup>19</sup> hydrogen and 8.80 x 10<sup>18</sup> helium atoms per year, respectively. These values correspond to 334 and 104 appm per year, respectively, and are consistent with values obtained by Abdou and Conn<sup>13</sup> in their comparison of radiation damage in several first-wall materials. At the higher wall loading, the dpa and gas-production rates are still low in the TF-coil windings.

Conclusions

The energy production and conversion systems aspects of the ORNL-EPR described in the text were developed from a broad scoping study performed previously. Detailed physics and engineering design lie ahead. The effort thus far has been to locate the EFP in a very complex multi-dimensional parameter space. This task is complete. The EPR as described will be capable of producing several hundred thermal megawatts. With scaling marginally improved beyond that presently predicted, a demonstration of breakeven will be achieved. The blanket, shield and cooling systems are sufficient to make the heat available at a high temperature datum and to shield the cryogenic systems from excessive inputs as well as provide suitable biological protection.

Acknowledgements

The authors express their gratitude to all the EPR design team participants. In particular, M. Roberts has continuously encouraged the work. Discussions with R. G. Alsmiller (Neutron Physics) and J. D. Callen (Thermonuclear Division) were most helpful.

References

1. N. A. Uckan, K. T. Tsang, J. D. Callen, "Toroidal Field Ripple Criteria for Large Tokamaks," paper #6, session A4, this Conference.
2. S. O. Dean, et al., USAEC Report Wash-1295 (1974).
3. N. P. Busharov, et al., "Chemical Sputtering of Graphite by H<sup>+</sup> Ions," I. V. Kurchatov Inst. Report, Moscow (1975) (in Russian).

4. D. M. Meade, et.al., "The Effects of Impurities and Magnetic Divertors on High Temperature Tokamaks," IAEA-CN-35/A15-4, Tokyo (1974).
5. R. Behrisch, Nuclear Fusion 12, 481 (1972).
6. W. W. Engle, Jr., "A Users Manual For ANISN, a One-Dimensional Discrete Ordinates Transport Code with Anisotropic Scattering," Report K-1683, Computing Technology Center, Union Carbide Corporation (1967).
7. D. M. Plaster, R. T. Santoro, and W. E. Ford, III, "Coupled 100-Group Neutron and 21-Group Gamma-Ray Cross Sections for EPR Calculations," ORNL-TM-4872, Oak Ridge National Laboratory (1975).
8. M. A. Abdou and R. W. Roussin, "MACKLEB - 100-Group Neutron Fluence-to-Kerma Factors and Reaction Cross Sections Generated by the MACK Computer Program from Data in ENDF Format," ORNL-TM-3995, Oak Ridge National Laboratory (1974).
9. N. M. Greene, et.al., "AMPX: A Modular Code System for Generating Coupled Multigroup Neutron-Gamma Libraries from ENDF/B," ORNL-TM-3705, Oak Ridge National Laboratory (to be published).
10. T. A. Gabriel, J. D. Amburgey, and N. M. Greene, Trans. Am. Nucl. Soc. 21, 67 (1975).
11. G. L. Kulcinski, D. G. Doran, and M. A. Abdou, "Comparison of the Displacement and Gas Production Rates in Current Fission and Future Fusion Reactors," preprint (1974).
12. M. L. Williams, R. T. Santoro, and T. A. Gabriel, "The Performance of Various Structural Materials in Fusion-Reactor Blankets," ORNL-TM-5036, Oak Ridge National Laboratory (in preparation).
13. M. A. Abdou and Robert W. Conn, "A Comparative Study of Several Fusion Reactor Blanket Designs," Nucl. Sci. Eng. 55, 256 (1974).

## Figure Captions

Figure 1. Fusion power outputs, temperature and neutron wall loading as a function of time.

Figure 2. Ion temperature vs. burn time (sputtering case).

Figure 3. Calculated temperature distribution in the reference design, at 5 azimuth locations. [Driven system - 400 MW (th)].

Figure 4. A schematic diagram of the EPR reference design used in the one-dimensional calculations.

Figure 5. The energy deposition vs. reactor radius.